

Breaking the Resolution Barrier: Arbitrary-resolution Deep Image Steganography Framework

Xinjue Hu¹, Chi Wang¹, Boyu Wang¹, Xiang Zhang¹, Zhenshan Tan¹ and Zhangjie Fu^{1*}

¹Engineering Research Center of Digital Forensics, Ministry of Education, Nanjing University of Information Science and Technology

{huxinjue, 202412200715, 202412200714, zhangxiang, zstan, fzj}@nuist.edu.cn

Abstract

Deep image steganography (DIS) has achieved significant results in capacity and invisibility. However, current paradigms enforce the secret image to maintain the same resolution as the cover image during hiding and revealing. This leads to two challenges: secret images with inconsistent resolutions must undergo resampling beforehand which results in detail loss during recovery, and the secret image cannot be recovered to its original resolution when the resolution value is unknown. To address these, we propose ARDIS, the first Arbitrary Resolution DIS framework, which shifts the paradigm from discrete mapping to reference-guided continuous signal reconstruction. Specifically, to minimize the detail loss caused by resolution mismatch, we first design a Frequency Decoupling Architecture in hiding stage. It disentangles the secret into a resolution-aligned global basis and a resolution-agnostic high-frequency latent to hide in a fixed-resolution cover. Second, for recovery, we propose a Latent-Guided Implicit Reconstructor to perform deterministic restoration. The recovered detail latent code modulates a continuous implicit function to accurately query and render high-frequency residuals onto the recovered global basis, ensuring faithful restoration of original details. Furthermore, to achieve blind recovery, we introduce an Implicit Resolution Coding strategy. By transforming discrete resolution values into dense feature maps and hiding them in the redundant space of the feature domain, the reconstructor can correctly decode the secret's resolution directly from the steganographic representation. Experimental results demonstrate that ARDIS significantly outperforms state-of-the-art methods in both invisibility and cross-resolution recovery fidelity.

1 Introduction

Deep image steganography aims to hide a secret image within a cover image imperceptibly while ensuring the receiver can

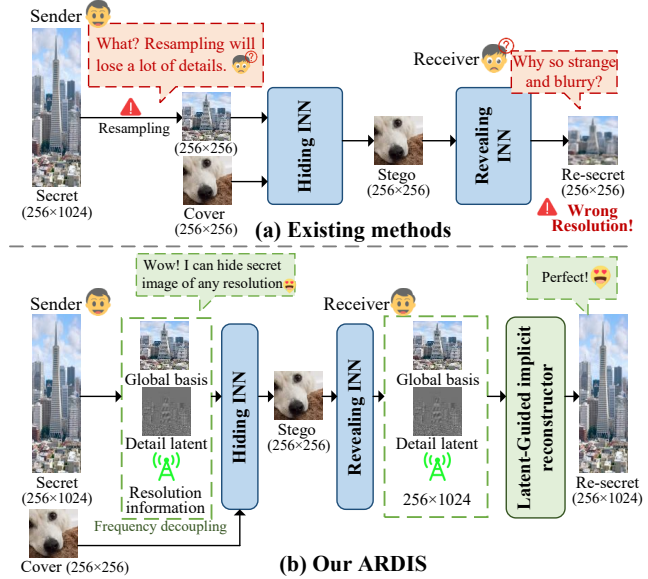


Figure 1: Overview of our ARDIS compared with existing methods. (a) Existing methods: The sender must manually resample the secret image to the same resolution as the cover image to hide it, and the recovered secret image will look strange due to the different resolution (e.g., different aspect ratio). (b) Our ARDIS enables arbitrary-resolution hiding and high-fidelity blind restoration.

recover the secret image with high fidelity. Due to its covert nature, it has been widely applied in copyright protection [Zhang *et al.*, 2024a; Zhang *et al.*, 2024b], digital forensics [Zhang *et al.*, 2025], military communications [Wani *et al.*, 2022], etc.

Existing DIS methods are mainly based on three architectures. Autoencoder-based methods [Baluja, 2017] rely on end-to-end encoder-decoder networks, which are prone to information loss due to repeated downsampling or non-linear transformations. Methods based on invertible neural networks (INNs) [Lu *et al.*, 2021] model the hiding and revealing of the secret image as a pair of bijective mappings with shared parameters, which theoretically avoids information loss and thus enables near-lossless high-quality hiding. Recently, some works have introduced diffusion models [Ho *et al.*, 2020a] into steganography [Yu *et al.*, 2023], using

*Corresponding authors.

prompts to guide the hiding and revealing process. However, their random sampling nature often limits pixel-level reconstruction accuracy.

Despite their architectural differences, existing methods share a critical limitation: the **fixed-resolution constraint**. They formulate DIS as a discrete pixel-mapping problem, learning local mappings on spatially aligned pixels. This paradigm requires the secret and cover images to own the same dimension. This constraint presents two challenges in real-world applications, as shown in Figure 1. **First, Resolution Mismatch Dilemma:** When the secret image differs in resolution from the cover, the sender must perform native resampling on the secret image, resulting in irreversible loss of high-frequency details in the recovered secret image. **Second, Blind Recovery Incapacity:** The receiver cannot obtain the resolution information of the secret image in advance, which means they can only recover a secret image with the same resolution as the cover image, but it is wrong. Relying on external transmission of metadata violates the principle of covert communication.

To bridge this gap, we propose ARDIS, the first Arbitrary-Resolution DIS framework. First, in order to solve the problem of detail loss caused by forced resampling under resolution mismatch at the sender side, our design is based on an intuitive idea: global low-frequency information is robust to resampling, but high-frequency details are highly susceptible. If they are processed as a whole, the fragile high-frequency details will inevitably be damaged due to resolution alignment constraints. Therefore, we propose frequency decoupling framework to decouple the secret image into a global visual basis and high-frequency detail latent information. The former characterizes global semantic cues and is aligned with the cover image’s resolution. The latter carries high-frequency residuals in a compressed, resolution-agnostic representation. This decoupling mechanism eliminates the impact of alignment constraints, ensuring that high-frequency details are not involved in lossy operations. Second, we find that the problem of lost detail in the recovered secret image caused by resolution mismatch stems from the limitations of the discrete pixel mapping paradigm: due to the limitations of fixed resolution, it must rely on interpolation operations when recovering secrets with wrong resolutions. To overcome this limitation, we shift the DIS paradigm from discrete pixel mapping to reference-guided continuous signal reconstruction, and design a latent-guided implicit reconstructor, which is a deterministic coordinate query in continuous space. We utilize the extracted high-frequency latent information as a conditional prior to modulate the implicit function, projecting the precise original high-frequency residuals onto the global basis to obtain a high-fidelity arbitrary-resolution secret image. Finally, to enable our reconstructor to perform blind recovery without violating steganography protocols, we introduce an implicit resolution encoding strategy. Simply hiding the resolution as a discrete scalar is extremely fragile, because the recovery process is not lossless, and small numerical fluctuations can lead to errors in resolution metadata. Therefore, we utilize the spatial redundancy of feature channels, broadcasting the resolution data into a dense feature map and embedding it, which provides a certain de-

gree of fault tolerance. The receiver can adaptively infer the correct original resolution from the stego image, eliminating the dependence on external metadata.

Our contributions can be summarized as follows:

1. To our knowledge, the proposed ARDIS is the first arbitrary-resolution DIS framework, effectively breaking the long-standing fixed-resolution constraint.
2. We design a frequency decoupling architecture for structure-detail separation of secret images at arbitrary resolutions. It encodes high-frequency textures that cannot be spatially aligned into a resolution-agnostic latent representation, thereby removing the dependence on cover-secret resolution alignment.
3. We propose a latent-guided implicit reconstructor that reformulates DIS recovery process as continuous image reconstruction based on a high-frequency detail latent, enabling high-fidelity texture recovery at arbitrary resolutions.
4. We introduce an implicit resolution coding strategy that leverages spatial redundancy in the feature domain to implicitly embed resolution priors, achieving geometry-consistent blind recovery when the secret resolution is unknown.

2 Related Work

Autoencoder-based DIS methods. Baluja [Baluja, 2017; Baluja, 2019] first introduced deep learning into image steganography, modeling the task as an end-to-end encoding-decoding process. Subsequent researchers have improved steganographic performance by designing various network architectures [Hayes and Danezis, 2017; Rahim *et al.*, 2018; Duan *et al.*, 2019; Yu, 2020; Zhang *et al.*, 2020; Ke *et al.*, 2024; Liu *et al.*, 2025]. However, since the parameters of the hiding and revealing networks are not shared, it is difficult to achieve a perfect balance between the visual imperceptibility of the stego image and the recovery fidelity of the secret image.

INNs-based DIS methods. To address the aforementioned trade-off, inspired by the success of Invertible Neural Networks (INNs) [Dinh *et al.*, 2014; Dinh *et al.*, 2016] in fields such as image translation [van der Ouderaa and Worrall, 2019], researchers have attempted to reconstruct the steganographic task by leveraging the strict invertibility of INNs [Lu *et al.*, 2021; Jing *et al.*, 2021; Xu *et al.*, 2022; Duan *et al.*, 2024; Li *et al.*, 2024; Luo *et al.*, 2024; Wang *et al.*, 2025; Zhou *et al.*, 2025]. For example, ISN [Lu *et al.*, 2021] first exploited this property to model the hiding and revealing processes as reciprocal mathematical transformations. HiNet [Jing *et al.*, 2021] further enhanced the hiding capacity for high-frequency information by incorporating wavelet transforms. Although these methods achieve near-lossless hiding and recovery, they strictly rely on the spatial alignment of input and output dimensions, rendering them incapable of handling cross-scale steganography scenarios with mismatched resolutions.

Diffusion-based DIS methods. Recently, with the rapid development of AIRC, Diffusion Models [Ho *et al.*, 2020b;

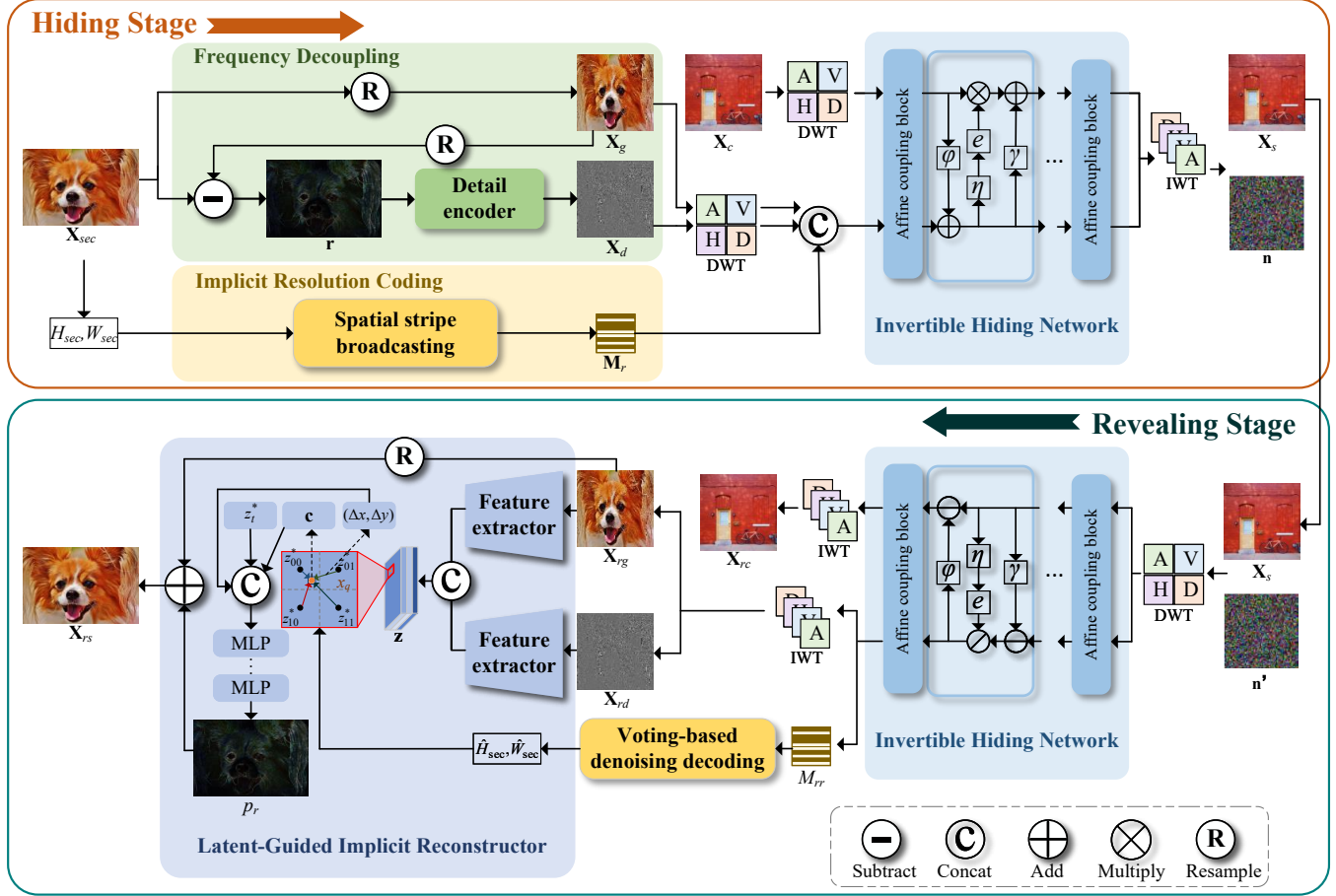


Figure 2: Overview of the proposed ARDIS, which supports hiding and revealing secret images at arbitrary resolutions.

Song *et al.*, 2020] have been introduced into the steganography domain due to their powerful capability in modeling data distributions. CRoSS [Yu *et al.*, 2023] leverages the randomness in the generation of diffusion models to design a training-free steganography scheme. DiffStega [Yang *et al.*, 2024] further added a preset password to avoid the risk of text prompts leaking information. However, diffusion models are fundamentally probabilistic generation processes, and their reverse sampling process possesses inherent randomness. This results in uncontrollable detail hallucinations or deviations during the recovery phase, making it difficult to achieve pixel-level precise restoration. Furthermore, these methods also fail to break free from the dependence on fixed resolutions.

3 Method

3.1 Overview

Our method consists of two stages: hiding and revealing. In hiding stage, shown in Figure 2 (top), we first decouple the arbitrary-resolution secret image \mathbf{X}_{sec} into a global visual basis \mathbf{X}_g , which matches the resolution of the cover \mathbf{X}_c , and a high-frequency detail latent code \mathbf{X}_d via the frequency decoupling architecture (FDA). Simultaneously, the spatial di-

mensions value (H_{sec}, W_{sec}) are encoded into a feature map \mathbf{M}_e via the implicit resolution coding strategy (IRC). \mathbf{X}_c , \mathbf{X}_g , and \mathbf{X}_d are converted into frequency features using discrete wavelet transform (DWT), and then fed along with \mathbf{M}_e into an invertible hiding network (IHN) consisting of a series of hidden blocks. The output of the last hidden block of the IHN is then go through an inverse wavelet transform (IWT) to generate the stego image \mathbf{X}_s and the lost information \mathbf{n} . In revealing stage, shown in Figure 2 (bottom), \mathbf{X}_s and auxiliary variable \mathbf{n}' are processed by DWT, inverse IHN, and IWT operations to obtain the recovered global visual basis \mathbf{X}_{rg} , detail latent code \mathbf{X}_{rd} , and resolution map \mathbf{M}_{re} . \mathbf{M}_{re} is decoded into the original dimensions via a resolution decoder. Subsequently, the recovered secret image \mathbf{X}_{rs} is reconstructed by latent-guided implicit reconstructor (LGIR). Explicitly conditioned on the detail latent, the reconstructor performs continuous spatial queries to predict fine-grained residuals p_r , enabling high-fidelity secret image reconstruction at arbitrary target resolutions. FDA, LGIR, and IRC are detailed in Sections 3.2, 3.3, and 3.4, respectively.

3.2 Frequency Decoupling Architecture

Frequency Decoupling Architecture (FDA) is designed to disentangle the secret into a resolution-aligned global basis and

a resolution-agnostic high-frequency latent code.

Formally, Given a secret image $\mathbf{X}_{sec} \in \mathbb{R}^{H_{sec} \times W_{sec} \times 3}$ and a cover image $\mathbf{X}_c \in \mathbb{R}^{H_c \times W_c \times 3}$, we define an adaptive resampling operator $\mathcal{R}(\mathbf{X}, (H, W))$, which can adjust the input $\mathbf{X} \in \mathbb{R}^{H_x \times W_x \times 3}$ to the target size (H, W) through bicubic interpolation. This operator can automatically perform downsampling (when $H_x > H$ or $W_x > W$) and upsampling (when $H_x < H$ or $W_x < W$) according to the actual situation. First, we extract the global visual basis \mathbf{X}_g :

$$\mathbf{X}_g = \mathcal{R}(\mathbf{X}_{sec}, (H_c, W_c)), \quad (1)$$

where \mathbf{X}_g is resolution-aligned with \mathbf{X}_c , preserving the basic global topological structure. It's worth noting that we choose explicit resampling over a general global extractor for this operation. This is because a learnable extractor introduces complex nonlinear global distortions, whereas resampling is a linear operation that strictly limits decoupled detail residuals to high frequencies and is spatially sparse. This is a prerequisite for subsequent detail encoding operations.

Then, we calculate the precise detail loss $\mathbf{r} \in \mathbb{R}^{H_{sec} \times W_{sec} \times 3}$:

$$\mathbf{r} = \mathbf{X}_{sec} - \mathcal{R}(\mathbf{X}_g, (H_{sec}, W_{sec})). \quad (2)$$

By explicitly resampling \mathbf{X}_g back to the original resolution and calculating the residual, we can precisely capture the pixel-level detail loss during the alignment process. \mathbf{r} is spatially sparse, mainly existing at edges and texture variations, thus it has high compressibility. Finally, we utilize a lightweight detail encoder E_{detail} to encode r into a compact high-frequency detail latent:

$$\mathbf{X}_d = E_{detail}(r), \quad (3)$$

where $\mathbf{X}_d \in \mathbb{R}^{H_c \times W_c \times c_{lat}}$. Through adaptive spatial processing, E_{detail} transforms the arbitrary-resolution \mathbf{r} into the fixed resolution latent. Although \mathbf{X}_d is spatially aligned with the cover for embedding, it is effectively used as a resolution-agnostic continuous prior for the subsequent reconstruction.

3.3 Latent-Guided Implicit Reconstructor

We propose Latent-Guided Implicit Reconstructor (LGIR), redefining the recovery process of the arbitrary-resolution secret image as a reference-guided deterministic continuous signal reconstruction, ensuring high-fidelity recovery of the secret image.

Inspired by Local Implicit Image Function (LIIF) [Chen *et al.*, 2021], we define a decoding function ϕ_θ to map continuous 2D coordinates $\mathbf{x} \in \mathbb{R}^2$ to RGB values $\mathbf{s} \in \mathbb{R}^3$ of the secret image:

$$\mathbf{s} = \phi_\theta(\mathbf{z}, \delta, c), \quad (4)$$

where $c = [\frac{2}{r_y H_{sec}}, \frac{2}{r_x W_{sec}}]$ is the cell decoding, r_y and r_x are variable scaling factors. δ represents the relative coordinate. \mathbf{z} is a feature vector, extracted differently from standard LIIF.

LIIF relies solely on low-resolution input to extract \mathbf{z} and infers missing details from blurred information. It only optimizes statistical plausibility rather than instance fidelity, inevitably introducing generic hallucinations. This constitutes a fatal flaw for deep image steganography which demands precise recovery. In contrast, we introduce the recovered detail latent code as a deterministic conditional mechanism:

$$\mathbf{z} = [\mathcal{E}_g(\mathbf{X}_{rg}), \mathcal{E}_d(\mathbf{X}_{rd})] \quad (5)$$

where \mathcal{E}_g and \mathcal{E}_d are feature encoder. Furthermore, in order to recover the original resolution secret image \mathbf{X}_{rs} , where the resolution is calculated by the resolution decoder in the IRC (mentioned in section 3.5), we define the query coordinates \mathbf{x}_q of \mathbf{X}_{rs} at the target resolution. The RGB value at \mathbf{x}_q can be reconstructed from the nearest surrounding latent codes $\mathbf{z}_t^*, t \in \{00, 01, 10, 11\}$,

$$\begin{aligned} \mathbf{X}_{rs}(\mathbf{x}_q) = & \sum_t \omega_t \phi_\theta(\mathbf{z}_t^*, \mathbf{x}_q - \mathbf{v}_t^*, c) \\ & + \mathcal{R}(\mathbf{X}_{rg}, (H_{sec}, W_{sec}))(\mathbf{x}_q), \end{aligned} \quad (6)$$

where \mathbf{v}_t^* is the coordinate of \mathbf{z}_t^* , ω_t is calculated based on the area of the rectangle formed by \mathbf{x}_q and \mathbf{v}_t^* , and satisfies $\sum_t \omega_t = 1$. This formulation explicitly compels the implicit function to synthesize missing textures guided by the detail latent, ensuring faithful restoration across continuous scales.

3.4 Implicit Resolution Coding Strategy

We propose an implicit resolution coding strategy (IRC) to address the problem that the receiver cannot recover the original resolution the secret image in blind recovery scenarios.

During the hiding stage, for the resolution (H_{sec}, W_{sec}) of the secret image, we first quantize it into a L-bit binary sequence $\mathbf{b} \in \{0, 1\}^L$. To resist potential distortion from subsequent IHN convolution operations, we design a spatial stripe broadcasting mechanism to generate a resolution feature map $\mathbf{M}_r \in \mathbb{R}^{\frac{H_c}{2} \times \frac{W_c}{2}}$. This map is spatially aligned with the cover features after DWT and is partitioned into L disjoint horizontal stripes, denoted as $\{\Omega_k\}_{k=1}^L$. For the k -th bit b_k in \mathbf{b} , we map it to a specific stripe region Ω_k in the \mathbf{M}_r :

$$\mathbf{M}_r(x, y) = 2b_k - 1, \quad \forall (x, y) \in \Omega_k. \quad (7)$$

where the mapped values are normalized to $\{-1, 1\}$, which ensures the zero-mean property, thus aligning with the underlying spatial distribution of the subsequent IHN.

During the revealing stage, since the recovered resolution map \mathbf{M}_{rr} contain some distortion ϵ , we design a voting-based denoising decoding mechanism:

$$\hat{b}_k = \mathbb{I} \left(\left(\frac{1}{|\Omega_k|} \sum_{(x,y) \in \Omega_k} \mathbf{M}_{rr}(x, y) \right) > 0 \right). \quad (8)$$

where $\mathbb{I}(\cdot)$ is defined as:

$$\mathbb{I}(\mathcal{C}) = \begin{cases} 1, & \text{if } \mathcal{C} \text{ is True} \\ 0, & \text{otherwise} \end{cases}. \quad (9)$$

Table 1: Controlled scaling performance evaluation results. ‘‘Blind Rec.’’ signifies the ability to recover the secret image without explicit resolution metadata. **It’s important to note that to calculate these visual metrics, we explicitly passed the resolution metadata to the contrastive methods that could not be blindly recovered. However, this is not permitted in real-world scenarios.**

Method	Venue	Blind Rec.	DIV2K												Avg. RRE% ↓					
			Res: 256 × 256				Res: 512 × 512				Res: 720 × 720									
			Stego		Resecret		Stego		Resecret		Stego		Resecret							
			PSNR↑	SSIM↑	PSNR↑	SSIM↑	PSNR↑	SSIM↑	PSNR↑	SSIM↑	PSNR↑	SSIM↑	PSNR↑	SSIM↑	PSNR↑					
ISN	CVPR’21	×	46.79	0.9938	42.98	0.9894	45.81	0.9922	27.88	0.8379	44.64	0.9896	26.05	0.7728	44.27	0.9885	24.80	0.7076	63.12	
HiNet	ICCV’21	×	41.69	0.9790	46.16	0.9942	39.80	0.9680	27.88	0.8400	37.73	0.9508	26.05	0.7739	37.14	0.9440	24.79	0.7083	63.12	
StegFormer	AAAI’24	×	47.21	0.9948	40.78	0.9924	47.02	0.9946	27.74	0.8361	46.68	0.9941	25.98	0.7725	46.56	0.9939	24.74	0.7085	63.12	
AIS	ICML’25	×	44.57	0.9574	33.22	0.8875	44.27	0.9566	26.33	0.7516	43.83	0.9535	24.67	0.6629	43.63	0.9522	23.63	0.6048	63.12	
ARDIS	-	✓	48.09	0.9951	48.39	0.9966	47.23	0.9940	30.93	0.8917	46.28	0.9923	28.08	0.8151	45.81	0.9913	26.63	0.7516	0	
Flickr2K																				
Method	Venue	Blind Rec.	Res: 256 × 256				Res: 512 × 512				Res: 720 × 720				Res: 1024 × 1024				Avg. RRE% ↓	
			Stego		Resecret		Stego		Resecret		Stego		Resecret		Stego		Resecret			
			PSNR↑	SSIM↑	PSNR↑	SSIM↑	PSNR↑	SSIM↑	PSNR↑	SSIM↑	PSNR↑	SSIM↑	PSNR↑	SSIM↑	PSNR↑	SSIM↑	PSNR↑	SSIM↑		
ISN	CVPR’21	×	46.60	0.9937	42.54	0.9858	45.66	0.9921	28.66	0.8501	44.57	0.9896	26.73	0.7909	44.19	0.9887	25.15	0.7218	63.12	
HiNet	ICCV’21	×	41.63	0.9781	45.86	0.9928	39.91	0.9680	28.72	0.8532	37.98	0.9518	26.76	0.7930	37.37	0.9469	25.17	0.7229	63.12	
StegFormer	AAAI’24	×	46.53	0.9933	40.90	0.9906	46.40	0.9931	28.44	0.8484	46.12	0.9926	26.60	0.7903	46.03	0.9924	25.07	0.7220	63.12	
AIS	ICML’25	×	44.35	0.9436	34.45	0.8811	44.18	0.9426	27.02	0.7620	43.82	0.9403	25.23	0.6821	43.67	0.9391	23.95	0.6202	63.12	
ARDIS	-	✓	47.68	0.9949	48.20	0.9960	46.93	0.9939	31.88	0.9022	46.13	0.9925	28.73	0.8304	45.73	0.9918	26.97	0.7636	0	

This mechanism performs collective voting and leverages the law of large numbers to cancel out randomly distributed distortion ϵ , thereby enabling bit-by-bit accurate recovery of \hat{b}_k . This ensures zero-error recovery of the original resolution $(\hat{H}_{sec}, \hat{W}_{sec})$ of the secret image.

4 Experiment

4.1 Datasets and Implementation Details

Implementation Details. We implement the framework using PyTorch on an NVIDIA Tesla V100 GPU. The training process employs the Adam optimizer with an initial learning rate of 10^{-4} and a Cosine Annealing decay schedule over 800 epochs. A channel-wise learnable clamp in IHN is initialized at 2.0 to stabilize high-frequency embedding. The MLP decoder in LGIR consists of 4 layers with a width of 256 using ReLU activations.

Evaluation Protocols. To establish an arbitrary resolution DIS evaluation benchmark, we constructed a multi-protocol evaluation benchmark to evaluate the invisibility of the stego image and the fidelity of the recovered secret image. We used four public datasets: DIV2K [Agustsson and Timofte, 2017], Flickr2K [Li et al., 2022], COCO [Lin et al., 2014], and Stego260 [Yu et al., 2023]. **Protocol-1: Controlled Resolution Performance Evaluation.** Based on DIV2K and Flickr2K, their high resolution supports dynamic cropping to simulate arbitrary resolution secrets without interpolation artifacts. In this protocol, the cover image is fixed at 256×256 resolution, and the secret image is cropped to four resolutions: 256×256 , 512×512 , 720×720 , and 1024×1024 . **Protocol-2: Generalization Evaluation in Complex Scenes.** Based on the COCO dataset, this evaluates the model’s adaptability to realistic, complex textured scenes and its ability to recover detail fidelity of the secret image across diverse image aspect ratios. In this protocol, the cover image is fixed at 256×256 resolution, while the secret image retains its original resolution. **Protocol-**

3: Domain-Specific Evaluation. Stego260 is used for a fair comparison with the diffusion-based DIS methods. This dataset is derived from public datasets [AISegment.cn, 2019; Banerjee, 2022] and the Google search engine and contains carefully crafted prompts from CRoSS. In this protocol, the cover image is fixed at 256×256 resolution and the secret image retains its original resolution.

Evaluation strategy. Since existing methods cannot perform blind recovery, we implement an asymmetric evaluation strategy: the contrasting methods are evaluated under settings that explicitly provide the true resolution, while our method is evaluated under a blind recovery setting. We used PSNR, SSIM, and LPIPS to evaluate hiding and recovery performance. Furthermore, we defined relative resolution error (RRE) specifically to evaluate our blind recovery capability:

$$RRE = \frac{1}{2} \left(\frac{|\hat{H} - H_{gt}|}{H_{gt}} + \frac{|\hat{W} - W_{gt}|}{W_{gt}} \right) \times 100\%. \quad (10)$$

where \hat{H} and \hat{W} are predicted resolution, H_{gt} and W_{gt} are ground-truth resolution.

Benchmarks. We compared the current state-of-the-art DIS methods, including ISN [Lu et al., 2021], HiNet [Jing et al., 2021], CRoSS [Yu et al., 2023], StegFormer [Ke et al., 2024], DiffStega [Yang et al., 2024], AIS [Zhou et al., 2025]. Among them, CRoSS and DiffStega are diffusion-based coverless DIS methods.

4.2 Experimental Results

Quantitative Results. In controlled resolution benchmarks, as shown in Table 1, maintains competitive invisibility for the stego image while exhibiting remarkable performance for the recovered secret image. This recovery superiority is particularly evident in the extreme scenario where the secret resolution is 1024×1024 , a setting where the effective payload amounts to 16x the cover’s spatial capacity. Despite this immense information density, ARDIS outperforms the second-best method by 1.83 dB in PSNR and 0.044 in SSIM on the

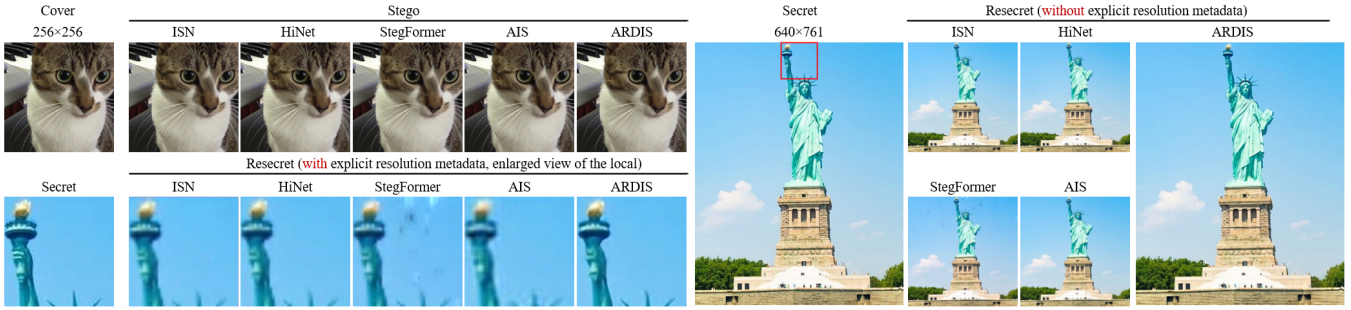


Figure 3: Visual comparisons of our ARDIS with leading deep image steganography methods for stego and recovering secret images in arbitrary-resolution hiding scenarios. The recovery of secret images presents two scenarios. (1) Without explicitly transmitting resolution metadata, no comparison methods can recover the secret image at the original resolution. (2) Explicitly transmitting resolution metadata, the comparison methods relies on resampling for recovery, which results in the loss of many details.

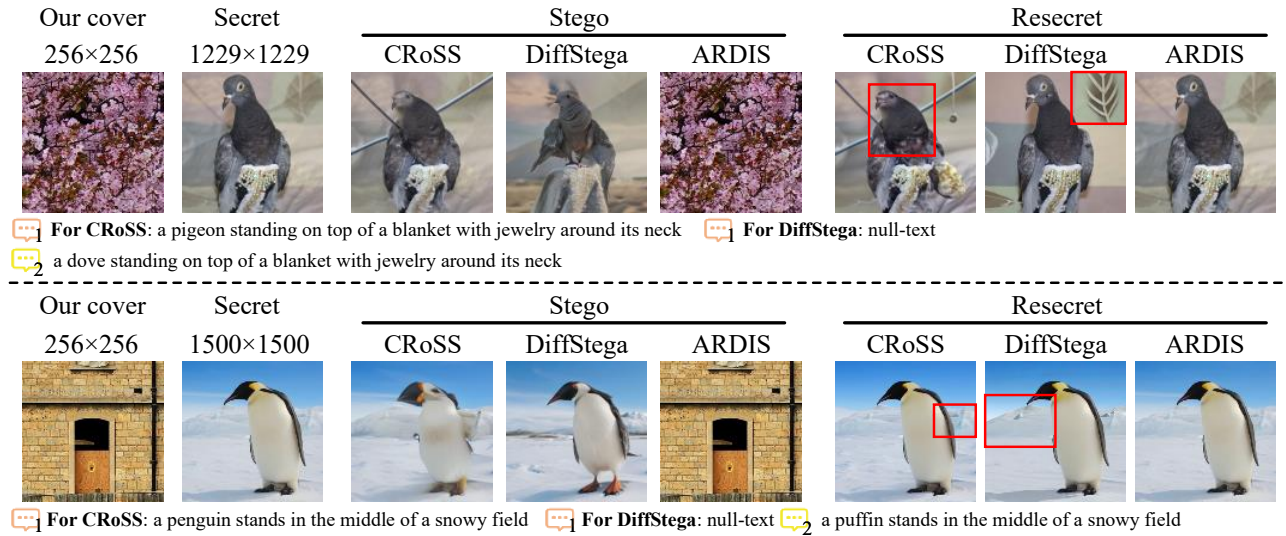


Figure 4: The visual comparison of ARDIS and the diffusion-based DIS method on the Stego260 dataset. The diffusion-based DIS method requires no cover and simply follows the prompts to generate the corresponding stego image. The settings for prompts 1 and 2 completely follow the design of the CRoSS and DiffStega methods.

DIV2K dataset. Crucially, ARDIS is the unique solution capable of blind recovery with a 0% RRE, while other methods can only recover secret images at the same resolution as the cover image, resulting in an RRE as high as 63.12%. Table 2 presents the results for generalization evaluation in complex scenes. ARDIS achieves dominant performance across both hiding and revealing stages by securing state-of-the-art results in PSNR, SSIM, and LPIPS simultaneously. This comprehensive superiority confirms that ARDIS recover complex real-world textures significantly better than existing approaches. Finally, results for domain-specific evaluation in Table 3 confirm a fundamental advantage over diffusion-based paradigms. For recovery secret images, ARDIS surpasses diffusion-based DIS method such as DiffStega by over 8 dB in PSNR. Furthermore, because the diffusion-based DIS method is coverless and requires a 512×512 input for the secret image, the RRE value differs from other comparison methods that cannot be blindly recovered.

Qualitative Results. Visual comparisons further demonstrate

Table 2: Generalization evaluation results.

Method	Venue	Blind Rec.	COCO						Avg RRE% ↓
			Stego			Resecret			
			PSNR↑	SSIM↑	LPIPS↓	PSNR↑	SSIM↑	LPIPS↓	
ISN	CVPR'21	✗	42.76	0.9873	0.0008	26.65	0.7954	0.2549	49.36
HiNet	ICCV'21	✗	37.22	0.9556	0.0026	26.67	0.7975	0.2540	49.36
StegFormer	AAAI'24	✗	41.99	0.9869	0.0008	26.51	0.7846	0.2549	49.36
AIS	ICML'25	✗	42.03	0.9254	0.0004	25.42	0.7022	0.4054	49.36
ARDIS	-	✓	42.65	0.9869	0.0002	28.70	0.8415	0.1115	0

the superiority of ARDIS. As shown in Figure 3, without explicitly informing the receiver of the secret image resolution, other comparison methods recover secret images with severe geometric distortions, such as the Statue of Liberty being incorrectly scaled. Even knowing the original resolution, the secret images recovered by comparison methods lose a significant amount of detail compared to ARDIS. Figure 4 reveals the limitations of diffusion-based methods (such as CRoSS and DiffStega), which are highly sensitive to prompts. With imperfectly designed prompts, the generated stego im-

Table 3: Domain-specific evaluation results. The resolutions of the secret image are from 225×225 to 3452×3452 .

Method	Venue	Blind Rec.	stego260						Avg. RRE%	
			Stego			Resecret				
			PSNR↑	SSIM↑	LPIPS↓	PSNR↑	SSIM↑	LPIPS↓		
ISN	CVPR'21	✗	46.62	0.9939	0.0006	30.87	0.8792	0.2153	62.83	
HiNet	ICCV'21	✗	41.05	0.9776	0.0011	30.98	0.8828	0.2172	62.83	
CRoSS	NeurIPS'23	✗	—	—	—	22.58	0.7308	0.2567	36.70	
StegFormer	AAAI'24	✗	46.52	0.9930	0.0005	30.66	0.8758	0.2169	62.83	
DiffStega	IJCAI'24	✗	—	—	—	24.67	0.7621	0.2110	36.70	
AIS	ICML'25	✗	44.36	0.9456	0.0004	29.48	0.8175	0.3009	62.83	
ARDIS	-	✓	48.01	0.9954	0.0001	32.89	0.9018	0.1091	0	

ages often exhibit obvious semantic distortions and unnatural traces. More critically, during the recovery stage, while the images generated by these methods may appear visually realistic, they actually contain textures completely unrelated to the original secret image. In contrast, ARDIS generates high-quality stego images while ensuring pixel-level consistency between the recovered results and the original secret image.

Security analysis. The anti-steganalysis ability is an important metric for evaluating the security of DIS methods. We assess the security of each method by exploring the number of leaked samples an attacker needs to effectively detect stego images [Weng *et al.*, 2019]. A detection accuracy closer to 50% indicates higher security. We train and test SRNet [Boroumand *et al.*, 2018] using cover / stego image pairs generated on the COCO dataset by our method or other comparison methods. As shown in Figure 5, our method maintains superior security even with an increase in leaked samples.

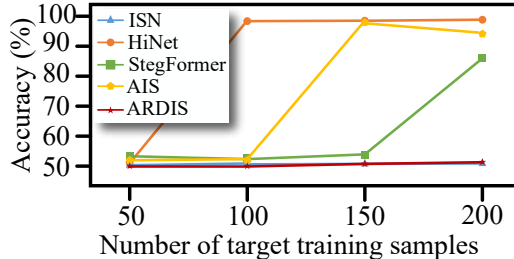


Figure 5: Steganalysis accuracy by SRNet. The fact that the curve remains close to 50% despite the increasing number of leaked samples demonstrates the high security of the method.

4.3 Ablation Study

To validate the effectiveness of each component in ARDIS, we conduct ablation experiments on COCO dataset. Results are shown in Table 4 and Fig. 6.

Effectiveness of FDA. FDA is essential to prevent information loss. Without it (#3), the secret image is naively resampled before hiding, causing irreversible high-frequency loss. Lacking deterministic detail guidance, the reconstructor produces results with noticeable artifacts or washed-out details, as illustrated in Fig. 6.

Effectiveness of LGIR. LGIR utilizes the decoupled latent for continuous and accurate reconstruction. As shown in Table 4, simply employing FDA without LGIR (#2) resulted in a performance improvement of only 0.19db compared to the baseline (#2). This indicates that standard resampling operators

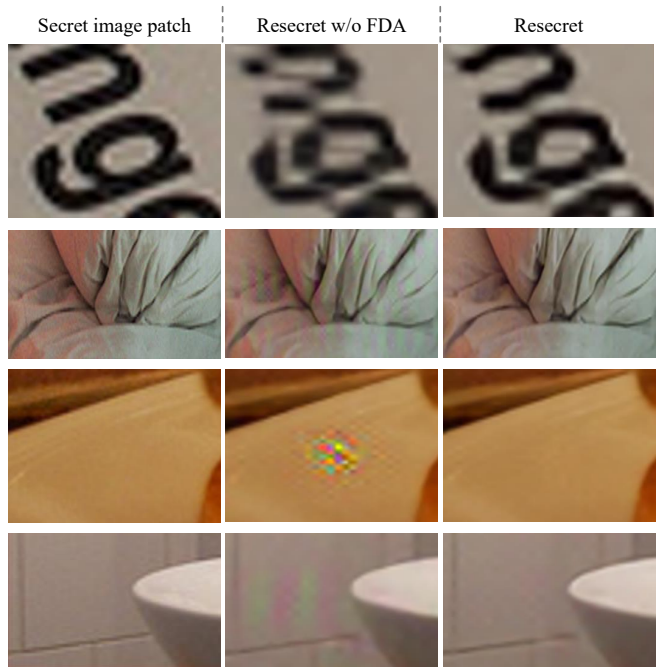


Figure 6: Impact of latent guidance on detail reconstruction. Without the FDA (“w/o FDA”), the reconstruction fails to resolve high-frequency textures, leading to over-smoothed edges and chromatic aberrations.

cannot effectively integrate the decoupled high-frequency latent. In contrast, introducing LGIR (#4) yields a 1.84 dB gain in recovery PSNR, which underscores the necessity of LGIR.

Table 4: Ablation experiments of different components

Variant	FDA	LGIR	COCO					
			Stego			Resecret		
PSNR↑	SSIM↑	LPIPS↓	PSNR↑	SSIM↑	LPIPS↓			
#1	✗	✗	42.35	0.9863	0.0003	27.18	0.8070	0.1654
#2	✓	✗	42.59	0.9872	0.0002	27.37	0.8108	0.1579
#3	✗	✓	40.48	0.9797	0.0004	28.27	0.8299	0.1276
#4	✓	✓	42.65	0.9869	0.0002	28.70	0.8415	0.1115

5 Conclusion

In this paper, we proposed **ARDIS**, the first framework to enable arbitrary-resolution deep image steganography. This work breaks the long-standing fixed-resolution constraint inherent in current DIS paradigms. Through the frequency decoupling architecture, ARDIS achieves the decoupled embedding of global structure and fine-grained detail during the hiding stage, guaranteeing the effective preservation of high-frequency information. Meanwhile, via the latent-guided implicit reconstructor, it ensures faithful and determinative detail restoration in the revealing stage. Furthermore, robust blind recovery is realized through the implicit resolution coding strategy. Experimental results demonstrate that ARDIS significantly outperforms state-of-the-art methods in both invisibility and cross-resolution recovery fidelity.

References

[Agustsson and Timofte, 2017] Eirikur Agustsson and Radu Timofte. Ntire 2017 challenge on single image super-resolution: Dataset and study. In *Proceedings of the IEEE conference on computer vision and pattern recognition workshops*, pages 126–135, 2017.

[AISegment.cn, 2019] AISegment.cn. Matting human datasets. https://github.com/aisegmentcn/matting_human-datasets, 2019.

[Baluja, 2017] Shumeet Baluja. Hiding images in plain sight: Deep steganography. *Advances in neural information processing systems*, 30, 2017.

[Baluja, 2019] Shumeet Baluja. Hiding images within images. *IEEE transactions on pattern analysis and machine intelligence*, 42(7):1685–1697, 2019.

[Banerjee, 2022] Sourav Banerjee. Animal image dataset (90 different animals). <https://www.kaggle.com/datasets/iamsouravbanerjee/animal-image-dataset-90-different-animals>, 2022.

[Boroumand *et al.*, 2018] Mehdi Boroumand, Mo Chen, and Jessica Fridrich. Deep residual network for steganalysis of digital images. *IEEE Transactions on Information Forensics and Security*, 14(5):1181–1193, 2018.

[Chen *et al.*, 2021] Yinbo Chen, Sifei Liu, and Xiaolong Wang. Learning continuous image representation with local implicit image function. In *Proceedings of the IEEE/CVF conference on computer vision and pattern recognition*, pages 8628–8638, 2021.

[Dinh *et al.*, 2014] Laurent Dinh, David Krueger, and Yoshua Bengio. Nice: Non-linear independent components estimation. *arXiv preprint arXiv:1410.8516*, 2014.

[Dinh *et al.*, 2016] Laurent Dinh, Jascha Sohl-Dickstein, and Samy Bengio. Density estimation using real nvp. *arXiv preprint arXiv:1605.08803*, 2016.

[Duan *et al.*, 2019] Xintao Duan, Kai Jia, Baoxia Li, Daidou Guo, En Zhang, and Chuan Qin. Reversible image steganography scheme based on a u-net structure. *Ieee Access*, 7:9314–9323, 2019.

[Duan *et al.*, 2024] Delin Duan, Shuyuan Shen, Songsen Yu, Yibo Yuan, Qidong Zhou, Haojie Lv, and Huanjie Lin. Densejin: Dense depth image steganography model with joint invertible and noninvertible mechanisms. *IEEE Transactions on Circuits and Systems for Video Technology*, 2024.

[Hayes and Danezis, 2017] Jamie Hayes and George Danezis. Generating steganographic images via adversarial training. *Advances in neural information processing systems*, 30, 2017.

[Ho *et al.*, 2020a] Jonathan Ho, Ajay Jain, and Pieter Abbeel. Denoising diffusion probabilistic models. *Advances in neural information processing systems*, 33:6840–6851, 2020.

[Ho *et al.*, 2020b] Jonathan Ho, Ajay Jain, and Pieter Abbeel. Denoising diffusion probabilistic models. *Advances in neural information processing systems*, 33:6840–6851, 2020.

[Jing *et al.*, 2021] Junpeng Jing, Xin Deng, Mai Xu, Jianyi Wang, and Zhenyu Guan. Hinet: Deep image hiding by invertible network. In *Proceedings of the IEEE/CVF international conference on computer vision*, pages 4733–4742, 2021.

[Ke *et al.*, 2024] Xiao Ke, Huanqi Wu, and Wenzhong Guo. Stegformer: Rebuilding the glory of autoencoder-based steganography. In *Proceedings of the AAAI Conference on Artificial Intelligence*, volume 38, pages 2723–2731, 2024.

[Li *et al.*, 2022] Lei Li, Jingzhu Tang, Ming Chen, Shijie Zhao, Junlin Li, and Li Zhang. Multi-patch learning: looking more pixels in the training phase. In *European Conference on Computer Vision*, pages 549–560. Springer, 2022.

[Li *et al.*, 2024] Fengyong Li, Yang Sheng, Kui Wu, Chuan Qin, and Xinpeng Zhang. Lidinet: A lightweight deep invertible network for image-in-image steganography. *IEEE Transactions on Information Forensics and Security*, 2024.

[Lin *et al.*, 2014] Tsung-Yi Lin, Michael Maire, Serge Belongie, James Hays, Pietro Perona, Deva Ramanan, Piotr Dollár, and C Lawrence Zitnick. Microsoft coco: Common objects in context. In *European conference on computer vision*, pages 740–755. Springer, 2014.

[Liu *et al.*, 2025] Hao Liu, Fengyong Li, Chuan Qin, and Xinpeng Zhang. Fearless of noise: Robust image-in-image hiding using dual-tree complex wavelet transform and state space model. *IEEE Transactions on Circuits and Systems for Video Technology*, 2025.

[Lu *et al.*, 2021] Shao-Ping Lu, Rong Wang, Tao Zhong, and Paul L Rosin. Large-capacity image steganography based on invertible neural networks. In *Proceedings of the IEEE/CVF conference on computer vision and pattern recognition*, pages 10816–10825, 2021.

[Luo *et al.*, 2024] Ting Luo, Yuhang Zhou, Zhouyan He, Gangyi Jiang, Haiyong Xu, Shuren Qi, and Yushu Zhang. Stegmamba: Distortion-free immune-cover for multi-image steganography with state space model. *IEEE Transactions on Circuits and Systems for Video Technology*, 2024.

[Rahim *et al.*, 2018] Rafia Rahim, Shahroz Nadeem, et al. End-to-end trained cnn encoder-decoder networks for image steganography. In *Proceedings of the European conference on computer vision (ECCV) workshops*, pages 0–0, 2018.

[Song *et al.*, 2020] Jiaming Song, Chenlin Meng, and Stefano Ermon. Denoising diffusion implicit models. *arXiv preprint arXiv:2010.02502*, 2020.

[van der Ouderaa and Worrall, 2019] Tycho FA van der Ouderaa and Daniel E Worrall. Reversible gans for memory-efficient image-to-image translation. In *Proceedings of the IEEE/CVF Conference on Computer Vision and Pattern Recognition*, pages 4720–4728, 2019.

[Wang *et al.*, 2025] Jiannian Wang, Yao Lu, and Guangming Lu. Sshr: More secure generative steganography with high-quality revealed secret images. In *Forty-second International Conference on Machine Learning*, 2025.

[Wani *et al.*, 2022] Pratik Wani, Anuja Nanaware, Sneha Shirode, Aishwarya Suram, and Archana Jadhav. Secret communication using multi-image steganography for military purposes. *International Journal of Advanced Research in Science, Communication and Technology*, 2, 2022.

[Weng *et al.*, 2019] Xinyu Weng, Yongzhi Li, Lu Chi, and Yadong Mu. High-capacity convolutional video steganography with temporal residual modeling. In *Proceedings of the 2019 on international conference on multimedia retrieval*, pages 87–95, 2019.

[Xu *et al.*, 2022] Youmin Xu, Chong Mou, Yujie Hu, Jingfen Xie, and Jian Zhang. Robust invertible image steganography. In *Proceedings of the IEEE/CVF conference on computer vision and pattern recognition*, pages 7875–7884, 2022.

[Yang *et al.*, 2024] Yiwei Yang, Zheyuan Liu, Jun Jia, Zhongpai Gao, Yunhao Li, Wei Sun, Xiaohong Liu, and Guangtao Zhai. Diffstega: towards universal training-free coverless image steganography with diffusion models. In *Proceedings of the Thirty-Third International Joint Conference on Artificial Intelligence*, pages 1579–1587, 2024.

[Yu *et al.*, 2023] Jiwen Yu, Xuanyu Zhang, Youmin Xu, and Jian Zhang. Cross: Diffusion model makes controllable, robust and secure image steganography. *Advances in Neural Information Processing Systems*, 36:80730–80743, 2023.

[Yu, 2020] Chong Yu. Attention based data hiding with generative adversarial networks. In *Proceedings of the AAAI conference on artificial intelligence*, volume 34, pages 1120–1128, 2020.

[Zhang *et al.*, 2020] Chaoning Zhang, Philipp Benz, Adil Karjauv, Geng Sun, and In So Kweon. Udh: Universal deep hiding for steganography, watermarking, and light field messaging. *Advances in Neural Information Processing Systems*, 33:10223–10234, 2020.

[Zhang *et al.*, 2024a] Xuanyu Zhang, Runyi Li, Jiwen Yu, Youmin Xu, Weiqi Li, and Jian Zhang. Editguard: Versatile image watermarking for tamper localization and copyright protection. In *Proceedings of the IEEE/CVF conference on computer vision and pattern recognition*, pages 11964–11974, 2024.

[Zhang *et al.*, 2024b] Yunming Zhang, Dengpan Ye, Caiyun Xie, Long Tang, Xin Liao, Ziyi Liu, Chuanxi Chen, and Jiacheng Deng. Dual defense: Adversarial, traceable, and invisible robust watermarking against face swapping. *IEEE Transactions on Information Forensics and Security*, 19:4628–4641, 2024.

[Zhang *et al.*, 2025] Xuanyu Zhang, Zecheng Tang, Zhipei Xu, Runyi Li, Youmin Xu, Bin Chen, Feng Gao, and Jian Zhang. Omnidguard: Hybrid manipulation localization via augmented versatile deep image watermarking. In *Proceedings of the Computer Vision and Pattern Recognition Conference*, pages 3008–3018, 2025.

[Zhou *et al.*, 2025] Junchao Zhou, Yao Lu, Jie Wen, and Guangming Lu. Efficient and separate authentication image steganography network. In *Forty-second International Conference on Machine Learning*, 2025.